# Density Functional Study on the Mechanisms of the Reactions of Gas-Phase $OsO_n^+$ ($n = 1-4$) with Methane

Ganbing Zhang, Shuhua Li,* and Yuansheng Jiang

*Department of Chemistry, Lab of Mesoscopic Chemistry, Institute of Theoretical and Computational Chemistry, Nanjing University, Nanjing, 210093, People's Republic of China*

*Received January 15, 2004*

The sextet, quartet, and doublet potential energy surfaces (PESs) of the reactions of methane with gas-phase $OsO_n^+$ ($n$=1−4) have been explored via density functional calculations to investigate the mechanisms of these reactions. For the reactions of $OsO_n^+$ ($n$ = 1−2) with methane, the minimum energy reaction paths are found to involve two spin inversions in the entrance and exit channels. Specifically, they are most likely to proceed through the following steps: $^4OsO^+ + CH_4 \rightarrow {}^2OOsCH_4^+ \rightarrow {}^2OOs(H)CH_3^+ \rightarrow {}^2OOsH(H)(CH_2)^+ \rightarrow {}^4OOs(CH_2)^+ + H_2$; and $^4OsO_2^+ + CH_4 \rightarrow {}^2O(O)OsCH_4^+ \rightarrow {}^2O(O)Os(H)CH_3^+ \rightarrow {}^2O(HO)Os(CH_3)^+ \rightarrow {}^2O(HO)Os(H)(CH_2)^+ \rightarrow {}^2OOs(H_2O)(CH_2)^+ \rightarrow {}^4OOs(CH_2)^+ + H_2O$, respectively. Along the minimum energy pathway the exothermicity of the overall reaction would be 17.3 kcal/mol for $OsO^+ + CH_4 \rightarrow OOs(CH_2)^+ + H_2$, and 24.0 kcal/mol for $OsO_2^+ + CH_4 \rightarrow OOs(CH_2)^+ + H_2O$. For the reaction of $OsO_3^+$ with methane, it is found to be kinetically unfavorable at room temperature because the intermediate generated by the activation of the first C−H bond has a significantly positive Gibbs free energy relative to the reactants. For $OsO_4^+$, our calculations suggest that it can readily react with methane on the doublet PES by a direct hydrogen atom abstraction process, and the whole reaction is exothermic by 31.8 kcal/mol. These results agree with the experimental observation that $OsO_n^+$ ($n$ = 1−2, 4) can readily activate methane but $OsO_3^+$ cannot.



## 1. Introduction

The C−H bond activation and transformation of methane has attracted considerable attention in recent years because of its scientific and potential economic significance.[1−9] Conversion of methane to more practical chemicals is one of the long-term goals of chemists due to the decreasing resources of crude oil and shifting to the utilization of coal and natural gas, with methane as the main component.[1a,7,8]

Transition-metal oxides are common catalysts in oxidation processes. Practical conversion processes of hydrocarbons usually occur in condensed phase, in which reaction processes are complicated by the irregular structure of the active sites and other processes such as adsorption and diffusion. However, the intrinsic mechanistic details of the C−H bond activation can be readily obtained in the gas phase, which is free of many complicated factors such as solvent, surface inhomogeneity, and aggregation effects occurring on surfaces or

* To whom correspondence should be addressed. E-mail: shuhua@netra.nju.edu.cn. Fax: +86-25-83686467.

(1) (a) Schwarz, H.; Schröder, D. *Pure Appl. Chem*. **2000**, 72, 2319−2332, and references therein. (b) Schröder, D.; Schwarz, H. *Angew. Chem., Int. Ed. Engl.* **1995**, *34*, 1973−1995, and references therein. (c) Armentrout, P. B.; Beauchamp, J. L. *Acc. Chem. Res.* **1989**, *22*, 315−321. (d) Weisshaar, J. C. *Acc. Chem. Res.* **1993**, *26*, 213-219.

(2) (a) Irikura, K. K.; Beauchamp, J. L. *J. Am. Chem. Soc.* **1991**, *113*, 2769−2770. (b) Irikura, K. K.; Beauchamp, J. L. *J. Phys. Chem.* **1991**, *95*, 8344−8351.

(3) Schwarz, H. *Angew. Chem., Int. Ed. Engl.* **1991**, *30*, 820−821.

(4) (a) Hendrickx, M.; Ceulemans, M.; Gong, K.; Vanquickenborne, L. *J. Phys. Chem. A* **1997**, *101*, 2465−2470. (b) Yoshizawa, K.; Suzuki, A.; Yamabe, T. *J. Am. Chem. Soc.* **1999**, *121*, 5266−5273. (c) Yoshizawa, K. *J. Organomet. Chem*. **2001**, *635*, 100−109.

(5) (a) Blomberg, M. R. A.; Siegbahn, P. E. M.; Svensson, M. *J. Phys. Chem*. **1994**, *98*, 2062−2071. (b) Armentrout, P. B.; Sievers, M. R. *J. Phys. Chem. A* **2003**, *107*, 4396−4406.

(6) (a) Irikura, K. K.; Goddard, W. A., III *J. Am. Chem. Soc.* **1994**, *116*, 8733−8740. (b) Heinemann, C.; Hertwig, R. H.; Wesendrup, R.; Koch, W.; Schwarz, H. *J. Am. Chem. Soc.* **1995**, *117*, 495−500.

(7) (a) Crabtree, R. H. *Chem. Rev.* **1985**, *85*, 245−269. (b) Crabtree, R. H. *Chem. Rev.* **1995**, *95*, 987−1007. (c) Lunsford, J. H. *Catal. Today* **2000**, *63*, 165−174. (d) Rostrup-Nielsen, J. R. *Catal. Today* **2000**, *63*, 159−164. (e) Ueda, W. *Catal. Today* **2001**, *71*, 1. (f) Schulz, H. *Appl. Catal. A* **1999**, *186*, 3−12. (g) Wolf, E. E., Ed. *Methane Conversion by Oxidative Processes*; Van Nostrand Reinhold: New York, 1992. (h) Gesser, H. D.; Hunter, N. R.; Prakash, C. B. *Chem. Rev.* **1985**, *85*, 2235−244. (i) Labinger, J. A.; Bercaw, J. E. *Nature* **2002**, *417*, 507−513. (j) Periana, R. A.; Mironov, O.; Taube, D.; Bhalla, G.; Jones, C. *Science* **2003**, *301*, 814−818. (k) *Chem. Eng. News* **1993**, *71*, 27.

(8) (a) Arndtsen, B. A.; Bergman, R. G.; Mobley, T. A.; Peterson, T. H. *Acc. Chem. Res.* **1995**, *28*, 154. (b) Shilov, A. E.; Shul'pin, G. B. *Chem. Rev.* **1997**, *97*, 2879−2932. (c) Sen, A. *Acc. Chem. Res.* **1998**, *31*, 550. (d) Periana, R. A.; Taube, D. J.; Gamble, S.; Taube, H.; Satoh, T.; Fujii, H. *Science* **1998**, *280*, 560. (e) Jones, W. D. *Science* **2000**, *287*, 1942. (f) Arakawa, H.; Aresta, M.; Armor, J. N.; Barteau, M. A.; Beckman, E. J.; Bell, A. T.; Bercaw, J. E.; Creutz, C.; Dinjus, E.; Dixon, D. A.; Domen, K.; Dubois, D. L.; Eckert, J.; Fujita, E.; Gibson, D. H.; Goddard, W. A., III; Goodman, D. W.; Keller, J.; Kubas, G. J.; Kung, H. H.; Lyons, J. E.; Manzer, L. E.; Marks, T. J.; Morokuma, K.; Nicholas, K. M.; Periana, R.; Que, L.; Rostrup-Nielson, J.; Sachtler, W. M. H.; Schmidt, L. D.; Sen, A.; Somorjai, G. A.; Stair, P. C.; Stults, B. R.; Tumas, W. *Chem. Rev.* **2001**, *101*, 953−996.

(9) (a) Saillard, J. Y.;Hoffmann, R. *J. Am. Chem.* Soc. **1984**, *106*, 2006−2026. (b) Choudhary, T. V.; Goodman, D. W. *J. Mol. Catal. A* **2000**, *163*, 9−18. (c) Liao, M.-S.; Au, C.-T.; Ng, C.-F. *Chem. Phys. Lett.* **1997**, *272*, 445−452. (d) Swang, O.; Faegri, K., Jr.; Gropen, O.; Wahlgren, U.; Siegbahn, P. *Chem. Phys.* **1991**, 156, 379−386. (e) Avdeev, V. I.; Zhidomirov, G. M. *Catal. Today* **1998**, *42*, 247−261. (f) Koga, N.; Morokuma, K. *J. Phys. Chem*. **1990**, *94*, 5454−5462. (g) Siegbahn, P. E. M.; Svensson, M. *J. Am. Chem*. Soc. **1994**, *116*, 10124−10128. (h) Basch, H.; Musave, D. G.; Mogi, K.; Morokuma, K. *J. Phys. Chem. A* **2001**, *105*, 3615−3622. (i) Cui, Q.; Musave, D. G.; Morokuma, K. *J. Chem. Phys.* **1998**, *108*, 8418. (j) Cui, Q.; Musave, D. G.; Morokuma, K. *J. Phys. Chem. A* **1998**, *102*, 6373.

10.1021/om049959b CCC: $27.50 
Publication on Web 06/19/2004

in solutions.[1−6,10] The effects of composition, stoichiometry, size, charge state, and degree of coordinative saturation, which are among the most important factors affecting catalytic properties, can be explored by employing gas-phase techniques. In recent years, the activation of small hydrocarbons such as methane by various transition-metal ions, transition-metal oxide ions, and transition-metal oxide cluster ions in the gas phase has received a great deal of attention both experimentally[1−3,11−19a] and theoretically.[4−6,16−30]

The product channels for first-, second-, and third-row analogues of cationic osmium oxides reacting with methane exhibit diversity. For example, $FeO^+$, the first-row congener of $OsO^+$, reacts with methane to give the products $FeOH^+ + {}^\bullet CH_3$, $Fe^+ + CH_3OH$, and $FeCH_2^+ + H_2O$, with the product-branching ratio [%] of 57/41/2, but $OsO^+$ can only dehydrogenate methane. $PtO^+$ reacts with methane at the collisional limit to yield $Pt(CH_2)^+$ and $H_2O$ as predominant products, whereas its first-row congener $NiO^+$ gives rise to $Ni^+$ and methanol only.[1a,b]

Up to now, many theoretical investigations on the mechanisms of the reactions of bare metal and monomeric metal oxide ions ($MO^+$) with $CH_4$ have been reported. The detailed PESs have been obtained for $ScO^+$,[30a] $TiO^+$,[30a] $VO^+$,[30a] $CrO^+$,[30a] $MnO^+$,[30a,c,31] $FeO^+$ [30] and $FeO^{2+}$,[30d] $CoO^+$,[30a,c] $NiO^+$,[30a] $CuO^+$,[30a] $PtO^+$[16b] with $CH_4$ to produce methanol or methyl. To our knowledge, there have been few theoretical studies on the activation of methane by second- and third-row transition-metal oxide ions and metal oxide cluster ions. Specifically, dehydrogenation or dehydration of methane by osmium oxide cations has not been theoretically explored.

On the other hand, numerous experimental studies on effects of ligands and oxidation states or charges of a transition metal on the gas-phase reactivity have been performed.[1b,32] For example, previous work has shown that the oxo ligand increases the reactivity for some diatomic transition-metal oxide ions, such as $CrO^+$, $MnO^+$, $FeO^+$, and $OsO^+$, but for the early transition metals, Sc, Ti, and V, the oxidation of the metal suppresses the reactivity relative to the bare metal ions. The overall reactivity of these $MO^+$ species is inversely correlated with their stability.[32j] Irikura and Beauchamp found that the number of oxo ligands has a striking effect on the chemistry of osmium oxide cluster ions. In particular, oxo ligands affect not only the reactivity but also the reaction pathways, which are presented as follows (where $\Phi$ denotes the reaction efficiency).[12]

$$Os^+ + CH_4 \xrightarrow{\Phi = 0.3} Os(CH_2)^+ + H_2 \quad (1)$$

$$OsO^+ + CH_4 \xrightarrow{\Phi = 0.6} OOs(CH_2)^+ + H_2 \quad (2)$$

$$OsO_2^+ + CH_4 \xrightarrow{\Phi = 0.5} OOs(CH_2)^+ + H_2O \quad (3)$$

$$OsO_3^+ + CH_4 \xrightarrow{\times} \quad (4)$$

$$OsO_4^+ + CH_4 \xrightarrow{\Phi = 0.7} OsO_3(OH)^+ + {}^\bullet CH_3 \quad (5)$$

We have investigated the mechanism of reaction 1, and detailed PESs in various multiplicities have been obtained theoretically.[33] To gain an insight into the effects of oxo ligands and oxidation states of the osmium center on the reactivities, we present here theoretical studies on the mechanisms of the reactions 2−5.

In recent years the density functional method, specifically the hybrid density functional B3LYP,[34] is proved to be a reliable tool for describing complicated electronic structures in open-shell transition-metal chemistry. We



(10) (a) Allison, J.; Freas, R. B.; Ridge, D. P. *J. Am. Chem. Soc.* **1979**, *101*, 1332−1333. (b) Eller, K.; Schwarz, H. *Chem. Rev.* **1991**, *91*, 1121−1177. (c) Armentrout, P. B. *Science* **1991**, *251*, 175−179.
(11) (a) Buckner, S. W.; McMahon, T. J.; Byrd, G. D.; Freiser, B. S. *Inorg. Chem.* **1989**, *28*, 3511−3518. (b) Ranasinghe, Y. A.; MacMahon, T. J.; Freiser, B. S. *J. Phys. Chem.* **1991**, *95*, 7721−7726.
(12) Irikura, K. K.; Beauchamp, J. L. *J. Am. Chem. Soc.* **1989**, *111*, 75−85.
(13) Sunderlin, L. S.; Armentrout, P. B. *J. Am. Chem.* Soc. **1989**, *111*, 3845−3855.
(14) Mourgues, P.; Ferhati, A.; McMahon, T. B.; Ohanessian, G. *Organometallics* **1997**, *16*, 210−224.
(15) Wesendrup, R.; Schröder, D.; Schwarz, H. *Angew. Chem., Int. Ed. Engl.* **1994**, *33*, 1174−1176.
(16) (a) Heinemann, C.; Wesendrup, R.; Schwarz, H. *Chem. Phys. Lett.* **1995**, *239*, 75−83. (b) Pavlov, M.; Blomberg, M. R. A.; Siegbahn, P. E. M.; Wesendrup, R.; Heinemann, C.; Schwarz, H. *J. Phys. Chem. A* **1997**, *101*, 1567−1579. (c) Achatz, U.; Beyer, M.; Joos, S.; Fox, B. S.; Niedner-Schatteburg, G.; Bondybey, V. E. *J. Phys. Chem. A* **1999**, *103*, 8200−8206. (d) Zhang, X. G.; Liyanage, R.; Armentrout, P. B. *J. Am. Chem. Soc.* **2001**, *123*, 5563−5575. (e) Hada, M.; Nakatsuji, H.; Nakai, H.; Gyobu, S.; Miki, S. *J. Mol. Struct. (THEOCHEM)* **1993**, *281*, 207−212.
(17) Sievers, M. R.; Chen, Y. M.; Haynes, C. L.; Armentrout, P. M. *Int. J. Mass Spectrom.* **2000**, *195/196*, 149−170, and references therein.
(18) (a) van Koppen, P. A. M.; Kemper, P. R.; Bushnell, J. E.; Bowers, M. T. *J. Am. Chem. Soc.* **1995**, *117*, 2098−2099. (b) van Koppen, P. A. M.; Perry, J. K.; Kemper, P. R.; Bushnell, J. E.; Bowers, M. T. *Int. J. Mass Spectrom.* **1999**, *185/186/187*, 989−1001.
(19) (a) Zhang, Q.; Kemper, P. R.; Shin, S. K.; Bowers, M. T. *Int. J. Mass Spectrom.* **2001**, *204*, 281−294. (b) Haynes, C. L.; Armentrout, P. B.; Perry, J. K.; Goddard, W. A., III. *J. Phys. Chem.* **1995**, *99*, 6340−6346.
(20) (a) Musaev, D. G.; Morokuma, K. *J. Phys. Chem.* **1996**, *100*, 11600−11609. (b) Russo, N.; Sicilia, E. *J. Am. Chem. Soc.* **2001**, *123*, 2588−2596.
(21) Sicilia, E.; Russo, N. *J. Am. Chem. Soc.* **2002**, *124*, 1471−1480.
(22) (a) Rodriguez-Arias, E. N.; Rincon, L.; Ruette, F. *Organometallics* **1992**, *11*, 3677−3683. (b) Musaev, D. G.; Morokuma, K. *J. Chem. Phys.* **1994**, *101*, 10697−10707. (c) Hendrickx, M.; Gong, K.; Vanquickenborne, L. *J. Chem. Phys.* **1997**, *107*, 6299−6305. (d) Holthausen, M. C.; Fiedler, A.; Schwarz, H.; Koch, W. *Angew. Chem., Int. Ed. Engl.* **1995**, *34*, 2282−2285. (e) Holthausen, M. C.; Fiedler, A.; Schwarz, H.; Koch, W. *J. Phys. Chem.* **1996**, *100*, 6236−6242. (f) Holthausen, M. C.; Koch, W. *Helv. Chim. Acta* **1996**, *79*, 1939−1956.
(23) (a) Musaev, D. G.; Morokuma, K.; Koga, N.; Ngyen, K.; Gordon, M. S.; Cundari, T. R. *J. Phys. Chem.* **1993**, *97*, 11435−11444. (b) Hendrickx, M.; Ceulemans, M.; Vanquickenborne, L. *Chem. Phys. Lett.* **1996**, 257, 8−14. (c) Perry, J. K.; Ohanessian, G.; Goddard, W. A., III. *J. Phys. Chem.* **1993**, *97*, 5238−5245.
(24) Yi, S. S.; Blomberg, M. R. A.; Siegbahn, P. E. M.; Weisshaar, J. C. *J. Phys. Chem. A* **1998**, *102*, 395−411.
(25) (a) Musaev, D. G.; Koga, N.; Morokuma, K. *J. Phys. Chem.* **1993**, *97*, 4064−4075. (b) Westerberg, J.; Blomberg, M. R. A. *J. Phys. Chem. A* **1998**, *102*, 7303−7307.
(26) Abashkin, Y. G.; Burt, S. K.; Russo, N. *J. Phys. Chem. A* **1997**, *101*, 8085−8093.
(27) Musaev, D. G.; Morokuma, K. *Isr. J. Chem.* **1993**, *33*, 307.
(28) (a) Sändig, N.; Koch, W. *Organometallics* **1997**, *16*, 5244−5251. (b) Sändig, N.; Koch, W. *Organometallics* **1998**, *17*, 2344−2351.
(29) Perry, J. K.; Ohanessian, G.; Goddard, W. A., III. *Organometallics* **1994**, *13*, 1870−1877.
(30) (a) Shiota, Y.; Yoshizawa, K. *J. Am. Chem. Soc.* **2000**, *122*, 12317−12326. (b) Yoshizawa, K.; Shiota, Y.; Yamabe, T. *Chem. Eur. J.* **1997**, *3*, 1160−1169. (c) Yoshizawa, K.; Shiota, Y.; Yamabe, T. *J. Am. Chem. Soc.* **1998**, *120*, 564−572. (d) Yoshizawa, K.; Shiota, Y.; Yamabe, T. *Organometallics* **1998**, *17*, 2825−2831. (e) Yoshizawa, K.; Shiota, Y.; Kagawa, Y.; Yamabe, T. *J. Phys. Chem. A* **2000**, *104*, 2552−2561. (f) Shiota, Y.; Yoshizawa, K. *J. Chem. Phys.* **2003**, *118*, 5872−5879. (g) Yoshizawa, K.; Shiota, Y.; Yamabe, T. *J. Chem. Phys.* **1999**, *111*, 538−545.
(31) Ryan, M. F.; Fiedler, A.; Schröder, D.; Schwarz, H. *J. Am. Chem. Soc.* **1995**, *117*, 2033−2040.

use the B3LYP method to investigate the detailed PESs of the reactions 2−5 in various spin multiplicities.

## 2. Computational Details

The spin-unrestricted density functional theory (UDFT) method based on the hybrid of Becke's three-parameter exchange functional[34b,c] and the Lee, Yang, and Parr correlation functional[34d] (B3LYP) has been used to carry out full optimization of geometries and energy calculations for all stationary points involved in the reactions. In all calculations, for osmium a relativistic effective core potential (RECP)[35] is employed for replacing the chemically inert 60 core electrons ([Kr] $4d^{10}$ $4f^{14}$), and the 5s and 5p orbitals are treated explicitly along with the 5d, 6s, and 6p valence orbitals. The basis set for osmium is a modified LANL2DZ[36] double-ζ basis set plus an f-type polarization function,[37] (341/341/41/1), where the two outermost 6p functions of the standard LANL2DZ have been replaced by a (41) split of the optimized 6p function from Couty and Hall.[38] The standard triple-ζ 6-311G** basis set[39] of Pople and co-workers is used for carbon, hydrogen, and oxygen. Frequency calculations are performed for all stationary points to check whether the optimized geometry corresponds to a minimum or a transition state and to obtain the zero-point vibrational energies (ZPVE) and Gibbs free energies. The total energies of all species are obtained by taking unscaled zero-point energy corrections into account. Intrinsic reaction coordinates (IRCs)[40] are traced from a transition state toward both reactant and product directions using the algorithm developed by Gonzalez and Schlegel[41] in the mass-weighted internal coordinate system to verify whether the reactant and the product are really connected by the transition state. All calculations have been performed using Gaussian 98 program.[42]

In our recent paper we have carefully calibrated the accuracy of the selected method in describing $[Os, C, H_4]^+$ species.[33] Our results indicated that without the inclusion of the spin/orbit effect the selected method still gives a good description on the reaction $Os^+ + CH_4$. For species $[Os, O_n, C, H_4]^+$ involved in the present work, it is also important to have some information on the accuracy of the selected method. The ionization potential of $OsO_4$ is calculated to be 13.02 eV, which is very close to the experimental value 12.97 ± 0.12 eV from the mass spectrometric study.[43] Previous theoretical work[44] also showed that for the $OsO_4$ molecule the B3LYP results could give satisfactory descriptions on the geometry and vibrational frequencies, being in good agreement with CCSD(T) results and experimental data. Later in this paper we will take the dehydration of methane by $OsO^+$ as an example to further calibrate the selected method by comparison with the UCCSD(T) method. Our results showed that the potential energy profiles described by UB3LYP and UCCSD(T) are fairly close to each other. Therefore, the B3LYP method with the selected basis set should be reliable in computing the relative energies of the species involved in the title reactions. The neglect of spin−orbit effects should not change the qualitative features of the reaction mechanisms captured by the present study.

## 3. Results and Discussions

First of all, we calculate the changes of Gibbs free energies ($\Delta G_{298}$) for the reactions of oxo osmium cations with methane proceeding along various product channels. Since those reaction channels with large positive $\Delta G_{298}$ values will be thermodynamically unfavorable, they are excluded in the following discussions. Instead, we will focus on those reaction channels with small or negative $\Delta G_{298}$ values.

Since the spin crossing is often involved in the transition-metal-containing reactions,[45] the potential energy profiles for the sextet, quartet, and doublet states are investigated. For the sake of convenience, each species is labeled with its spin multiplicity as a superscript preceding the formula, while its spatial symmetry is omitted in the present context.

In addition, for the sake of conciseness, the relative energies of all species and the optimized geometries for those species in higher potential energy profiles are given in the Supporting Information.



(32) (a) Stöckigt, D.; Schwarz, H. *Chem. Ber.* **1994**, *127*, 2499−2503. (b) Schröder, D.; Schwarz, H. *Angew. Chem., Int. Ed. Engl.* **1991**, *30*, 991−994. (c) Stöckigt, D.; Schwarz, H. *Chem. Ber.* **1992**, *125*, 2817−2819. (d) Armentrout, P. B.; Tjelta, B. L. *Organometallics* **1997**, *16*, 5372−5374. (e) Kretzschmar, I.; Fiedler, A.; Harvey, J. N.; Schröder, D.; Schwarz, H. *J. Phys. Chem. A* **1997**, *101*, 6252−6264. (f) Kretzschmar, I.; Schröder, D.; Schwarz, H. *Int. J. Mass Spectrosc., Ion. Processes* **1997**, *167/168*, 103−115. (g) Kretzschmar, I.; Schröder, D.; Schwarz, H.; Armentrout, P. B. *Int. J. Mass Spectrosc.* **2003**, *228*, 439−456. (h) Siegbahn, P. E. M. *J. Organomet. Chem.* **1995**, *491*, 231−245. (i) Siegbahn, P. E. M.; Blomberg, M. R. A. *Organometallics* **1994**, 13, 354−363. (j) Clemmer, D. E.; Aristov, N.; Armentrout, P. B. *J. Phys. Chem.* **1993**, *97*, 544−552. (k) Jackson, T. C.; Carlin, T. J.; Freiser, B. S. *J. Am. Chem. Soc.* **1986**, *108*, 1120−1126. (l) Cornehl, H. H.; Wesendrup, R.; Harvey, J. N.; Schwarz, H. *J. Chem. Soc., Perkin Trans. 2* **1997**, 2283−2291. (m) Cornehl, H. H.; Wesendrup, R.; Diefenbach, M.; Schwarz, H. *Chem. Eur. J.* **1997**, *3*, 1083−1090. (n) Bell, B. C.; Zemski, K. A.; Castleman, A. W., Jr. *J. Phys. Chem. A* **1999**, *103*, 2992−2998. (o) Harvey, J. N.; Diefenbach, M.; Schröder, D.; Schwarz, H. *Int. J. Mass Spectrosc.* **1999**, *182/183*, 85−97. (p) Koyanagi, G. K.; Bohme, D.; Kretzschmar, I.; Schröder, D.; Schwarz, H. *J. Phys. Chem. A* **2001**, *105*, 4259−4271. (q) Cassady, C. J.; McElvany, S. W. *Organometallics* **1992**, *11*, 2367−2377. (r) Fialko, E. F.; Kikhtenko, A. V.; Goncharov, V. B.; Zamaraev, K. I. *J. Phys. Chem. A* **1997**, *101*, 8607−8613. (s) Zemski, K. A.; Bell, B. C.; Castleman, A. W., Jr. *J. Phys. Chem. A* **2000**, *104*, 5732−5741. (t) Zemski, K. A.; Justes, D. R.; Bell, B. C.; Castleman, A. W., Jr. *J. Phys. Chem. A* **2001**, *105*, 4410−4417. (u) Beyer, M. K.; Berg, C. B.; Bondybey, V. E. *Phys. Chem. Chem. Phys.* **2001**, *3*, 1840−1847.

(33) Zhang, G. B.; Li, S. H.; Jiang, Y. S. *Organometallics* **2003**, *22*, 3820−3830.

(34) (a) Stephens, P. J.; Devlin, F. J.; Chabalowski, C. F.; Frisch, M. J. *J. Phys. Chem.* **1994**, *98*, 11623−11627. (b) Becke, A. D. *Phys. Rev. A* **1998**, *38*, 3098−3100. (c) Becke, A. D. *J. Chem. Phys.* **1993**, *98*, 5648−5652. (d) Lee, C.; Yang, W.; Parr, R. G. *Phys. Rev. B* **1988**, *37*, 785−789.

(35) (a) Hay, P. J.; Wadt, W. R. *J. Chem. Phys.* **1985**, *82*, 270. (b) Wadt, W. R.; Hay, P. J. *J. Chem. Phys.* **1985**, *82*, 284. (c) Hay, P. J.; Wadt, W. R. *J. Chem. Phys.* **1985**, *82*, 299.

(36) LANL2DZ: Dunning D95 basis sets on first row, Los Alamos ECP plus double-ζ basis sets on Na−Bi.

(37) Ehlers, A. W.; Böhme, M.; Dapprich, S.; Gobbi, A.; Höllwarth, A.; Jonas, V.; Köhler, K. F.; Stegmann, R.; Veldkamp, A.; Frenking, G. *Chem. Phys. Lett.* **1993**, *208*, 111−114.

(38) Couty, M.; Hall, M. B. *J. Comput. Chem.* **1996**, *17*, 1359−1370.

(39) Krishnan, R.; Binkley, J. S.; Seeger, R.; Pople, J. A. *J. Chem. Phys.* **1980**, *72*, 650.

(40) (a) Fukui, K. *J. Phys. Chem.* **1970**, *74*, 4161−4163. (b) Fukui, K. *Acc. Chem. Res.* **1981**, *14*, 363−368.

(41) Gonzalez, C.; Schlegel, H. B. *J. Phys. Chem.* **1990**, *94*, 5523−5527.

(42) Frisch, M. J.; Trucks, G. W.; Schlegel, H. B.; Scuseria, G. E.; Robb, M. A.; Cheeseman, J. R. Zakrzewski, V. G.; Montgomery, J. A., Jr.; Stratmann, R. E.; Burant, J. C.; Dapprich, S.; Millam, J. M.; Daniels, A. D.; Kudin, K. N.; Strain, M. C.; Farkas, O.; Tomasi, J.; Barone, V.; Cossi, M.; Cammi, R.; Mennucci, B.; Pomelli, C.; Adamo, C.; Clifford, S.; Ochterski, J.; Petersson, G. A.; Ayala, P. Y.; Cui, Q.; Morokuma, K.; Malick, D. K.; Rabuck, A. D.; Raghavachari, K.; Foresman, J. B.; Cioslowski, J.; Ortiz, J. V.; Baboul, A. G.; Stefanov, B. B.; Liu, G.; Liashenko, A.; Piskorz, P.; Komaromi, I.; Gomperts, R.; Martin, R. L.; Fox, D. J.; Keith, T.; Al-Laham, M. A.; Peng, C. Y.; Nanayakkara, A.; Challacombe, M.; Gill, P. M. W.; Johnson, B.; Chen, W.; Wong, M. W.; Andres, J. L.; Gonzalez, C.; Head-Gordon, M.; Replogle, E. S.; Pople, J. A. *GAUSSIAN 98* (release A.9); Gaussian, Inc.: Pittsburgh, PA, 1998.

(43) Dillard, J. G.; Kiser, R. W. *J. Phys. Chem.* **1965**, *69*, 3893−3897.

(44) Ujaque, G.; Maseras, F.; Lled s, A. *Int. J. Quantum Chem.* **2000**, *77*, 544−551.

(45) (a) Shaik, S.; Danovich, D.; Fiedler, A.; Schröder, D.; Schwarz, H. *Helv. Chim. Acta* **1995**, *78*, 1393−1407. (b) Schröder, D.; Shaik, S.; Schwarz, H. *Acc. Chem. Res.* **2000**, *33*, 139−145.

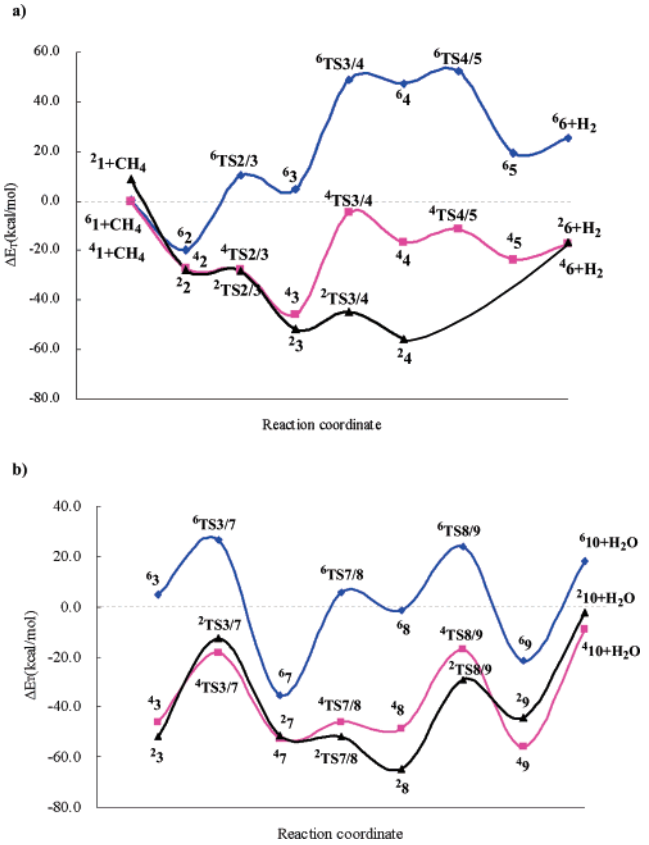


**Figure 1.** UB3LYP potential energy profiles of the reactions (a) $OsO^+ + CH_4 \rightarrow OOsCH_2^+ + H_2$ and (b) $OsO^+ + CH_4 \rightarrow OsCH_2^+ + H_2O$ in the sextet, quartet, and doublet states, respectively. The early part of the pathway b is the same as that of the pathway a. For all species, the energies ($E_T$) are the sum of electronic energies and zero-point vibrational energies.

**3.1. Reaction of $OsO^+$ with Methane.** According to calculations, dehydrogenation and dehydration channels are the thermodynamically possible processes for the reaction of $OsO^+$ with $CH_4$. For both reaction channels, the calculated potential energy profiles for the sextet, quartet, and doublet states are given in Figure 1, and the optimized geometries for all stationary points in the quartet and doublet states are presented in Figure 2. Since the dehydrogenation process was observed experimentally, we will discuss this channel first.

**3.1.1. $OsO^+ + CH_4 \rightarrow OOs(CH_2)^+ + H_2$.** From Figure 1a, the PESs in the sextet and quartet states for methane dehydrogenation by $OsO^+$ are very similar to each other, except that the sextet surface is higher in energy and the initial reactants in the sextet state are almost isoenergetic to those in the quartet state. One can see that methane dehydrogenation by $OsO^+$ is uphill in energy on the sextet surface, and the whole reaction on this path is endothermic by 24.7 kcal/mol. Thus, the reaction proceeding on the sextet surface is very unfavorable in energy. We will focus the discussions on the lower quartet and doublet surfaces.

As depicted in Figure 1a and Figure 2a, on the quartet reaction path, the initial step is the formation of the $\eta^2$-methane complex, $OOs(CH_4)^+$ ($^4$**2**), which is bound by 27.3 kcal/mol below the entrance channel $^4OOs^+ + CH_4$, followed by the oxidative addition of one C−H bond of methane to the metal to form the complex $OOs(H)CH_3^+$ ($^4$**3**) via the transition state $^4$**TS2/3**. This step has a very small barrier and is exothermic by 18.8 kcal/mol. The next step is the activation of the second C−H bond of methane through the transition state $^4$**TS3/4** to generate the methylene dihydride complex $(H)_2(O)Os(CH_2)^+$ ($^4$**4**), which is 29.1 kcal/mol higher in energy than $^4$**3** with a barrier of 41.2 kcal/mol. Then, the two hydrides bonded to the metal reductively eliminate to form the methylene dihydrogen complex $(H_2)(O)Os(CH_2)^+$ ($^4$**5**), with a low activation barrier of 5.6 kcal/mol. Finally, $^4$**5** would readily dissociate to produce the products $OOsCH_2^+$ ($^4$**6**) and $H_2$. One can see that the whole reaction on this path is exothermic by 17.3 kcal/mol on the quartet surface. The activation of the second C−H bond through the transition state $^4$**TS3/4** with a barrier of 41.2 kcal/mol is the slowest step on the quartet reaction path. Since the Gibbs free energy of $^4$**TS3/4** is even 2.8 kcal/mol higher than that of the quartet reactants $^4OsO^+ + CH_4$, this step does not occur easily at the room temperature. For convenience in later discussions, hereafter we use H1 and H2 to denote the first and second hydrogens of methane activated by $OsO^+$, respectively.

As shown in Figure 1a and Figure 2b, methane dehydrogenation by $OsO^+$ on the earlier part of the doublet path is very similar to that on the quartet one. Especially, the barrier of the first C−H activation step is very small for both doublet and quartet states. However, the evident differences between the latter parts of two paths exist. First, different from that on the quartet path, the oxidative addition of the second C−H bond to form the methylene dihydride oxo complex $^2$**4** is facile on the doublet path with a low barrier of only 6.7 kcal/mol. Second, the last step on the doublet path is the direct elimination of $H_2$ from $^2$**4** without the formation of the methylene dihydrogen oxo complex, $(H_2)(O)Os(CH_2)^+$. Numerous attempts to look for the doublet dihydrogen oxo complex failed. We also have performed constrained geometry optimizations by fixing the H−H distance at various values. The results showed that the energy ascends monotonically as the H−H distance decreases from 2.109Å in $^2$**4** to 0.740 Å in a free $H_2$. The rate-determining step on the doublet path is the elimination of $H_2$ from $^2$**4**, which requires 39.2 kcal/mol. Although this step is highly endothermic, it can couple with the preceding steps, which have a total exothermicity of 55.9 kcal/mol. The overall reaction on the doublet path is exothermic by 16.7 kcal/mol.

We can qualitatively understand the relative stability of some intermediates in different spin multiplicities. In $^2$**3** and $^4$**3**, the formal oxidation state of Os in each species is +5, and the bonding modes can be described as follows: in $^2$**3**, the $Os^+$ center provides four sd hybrid orbitals and four electrons to form normal covalent bonds Os−H, Os−C, and Os═O. For the other three electrons in two 5d orbitals, one orbital is doubly occupied and the other is singly occupied. Thus the bonding mode is optimal only if **3** is in the doublet state. If **3** is in the quartet state, there must be only two electrons in two 5d orbitals and consequently five electrons in the former three bonds, leading to a weak three-electron bond. As a consequence, $^2$**3** is more stable than $^4$**3**. Furthermore, in comparison with the formation of two typical covalent Os−H and Os−C bonds in species

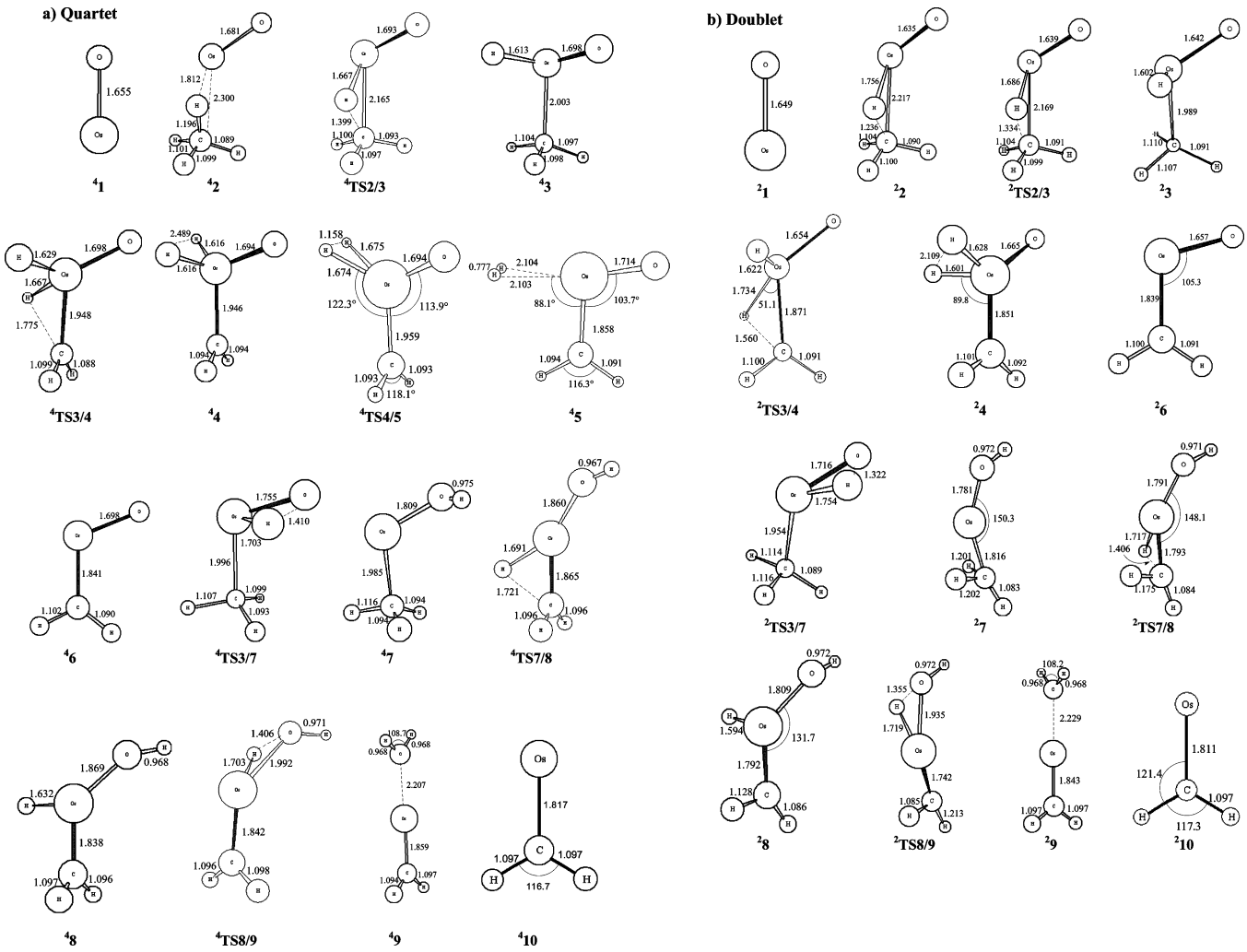


**Figure 2.** Optimized geometries for the stationary points of the reactions $OsO^+ + CH_4 \rightarrow OOsCH_2^+ + H_2$ and $OsO^+ + CH_4 \rightarrow OsCH_2^+ + H_2O$ in the quartet (a) and doublet (b) states.

$^2$**3** and $^4$**3**, only one typical covalent Os−H bond can be formed in $^6$**3** to meet the requirement of the sextet state. Thus, $^6$**3** has the highest energy in three spin states. Similarly, for species **4**, $^2$**4** has the optimal bonding mode due to the requirement of both the spin state and the formal oxidation state of Os; therefore it has the lowest energy in three species with different spin states.

To summarize, the reaction on the sextet path is unlikely to take place because of its strong endothermicity. Instead, the reaction on the quartet and doublet paths is thermodynamically possible, due to the exothermicity, 17.3 and 16.7 kcal/mol, respectively. However, since the rate-limiting step from $^4$**3** to $^4$**4** does not easily occur on the quartet surface, in the intermediate stages the reaction occurs more probably on the doublet surface than on the quartet surface.

As seen from Figures 1a and 2, the ground state of the reactants, $^4OsO^+ + CH_4$, is just 0.5 kcal/mol lower than the sextet species and lies 8.7 kcal/mol below the doublet species. The ground state of the final products is $^4$**6** + $CH_4$, which lies 0.6 and 42.5 kcal/mol below the corresponding doublet and sextet species, respectively. However, the intermediates and transition states (except the reactants and the products) are more stable on the doublet surface. If methane can be dehydrogenated readily by the ground-state $OsO^+$, as observed experimentally, there must be crossings between the doublet and quartet surfaces, caused by the spin−orbit coupling. From Figure 1a, the surface crossings may occur twice. The first one occurs between the doublet and quartet (or sextet) surfaces near the entrance channel, and the second crossing occurs near the exit channel. Since the energy difference between $^4$**6** and $^2$**6** is very small, the product **6** may exist in both spin states.

**3.1.2. $OsO^+ + CH_4 \rightarrow Os(CH_2)^+ + H_2O$.** For this reaction channel, its PESs in three spin states are shown in Figure 1b. Most of the stationary points on the sextet surface are much higher in energy than those on quartet and doublet surfaces, except that the sextet initial reactant is isoenergetic to the corresponding quartet species and lower in energy than the corresponding doublet species. Hence, we will give a brief discussion on the quartet and doublet reaction pathways.

As seen from Figure 1b, the PESs of the dehydration reaction diverge from those of the dehydrogenation reaction after the intermediate **3** is formed. Along the dehydration direction, the subsequent step is the migration of the hydride from Os to the oxo ligand to yield the hydroxyl complex $Os(OH)(CH_3)^+$ (**7**) via **TS3/7**. Next, the second C−H bond of methane oxidatively adds to the metal to form the intermediate $Os(H)(OH)(CH_2)^+$ (**8**). Then a reductive elimination step with H2 shifting

from Os to the newly formed hydroxyl ligand occurs, forming a water-coordinated complex $Os(H_2O)(CH_2)^+$ (**9**). Finally, **9** releases the water to give the final products $Os(CH_2)^+$ (**10**) + $H_2O$.

The results show that the steps of the first and second C−H oxidative addition in both quartet and doublet states have low barriers, but two reductive elimination steps and the step involving the loss of the water ligand have relatively high barriers. Since the ground states of the initial reactant $OsO^+$, the final product $Os(CH_2)^+$, and intermediates **7** and **9** are in the quartet state, other species have the lowest energies on the doublet surface. There must be crossings between the quartet and doublet surfaces, caused by the spin−orbit coupling. After taking the spin crossings into account, it is expected that the barriers of two reductive elimination steps could be reduced to some extent. Thermodynamically, the entire reaction for the dehydration of methane by $OsO^+$ is exothermic by about 9.0 kcal/mol and thus may occur.

Comparing the dehydration and dehydrogenation reaction channels, one can see that the final products of the dehydration reaction are 8.3 kcal/mol higher in energy than those of the dehydrogenation reaction described above. Thus the dehydrogenation channel is thermodynamically more favorable. On the other hand, since the hydride transfer step from **3** to **7** along the dehydration path has a much higher barrier than the second C−H oxidative addition step on the dehydrogenation path, the dehydrogenation channel is also preferred kinetically. Under the conditions that both reaction channels are thermodynamically accessible, what really distinguishes these two pathways is the kinetic difference. Thus the dehydrogenation channel is favored, which is in agreement with the experimental result that $H_2$ not $H_2O$ was observed in the final products.

To conclude, the reaction of $OsO^+$ with methane will prefer to proceed through the dehydrogenation channel. If the reaction goes on the minimum energy path, two possible spin crossings are involved in the process. First, the reaction may start on the quartet surface. Then, the quartet surface should cross the doublet surface somewhere before the formation of the encounter complex $^2$**2**. After $^2$**4** is formed, the reaction may jump back to the quartet surface in the exit channel. The minimum energy pathway may be described as $^4OsO^+ + CH_4 \rightarrow OOsCH_4^+$ ($^2$**2**) → $OOs(H)(CH_3)^+$ ($^2$**3**) → $OOs(H)_2(CH_2)^+$ ($^2$**4**) → $OOs(CH_2)^+$ ($^4$**6**) + $H_2$. If the reaction starts on the quartet PES and ends on the quartet PES, the overall reaction would be exothermic by 17.3 kcal/mol. If the reaction ends up with the doublet product (almost isoenergetic to the quartet product), the total reaction would be exothermic by 16.7 kcal/mol. Thus, no matter what spin state the final product $OOs(CH_2)^+$ is in, our results can rationalize the experimental fact that methane can be dehydrogenated by $OsO^+$.

As seen from Figure 1b, the quartet and doublet PESs along the dehydration channel are quite close to each other. To check whether the B3LYP method reasonably describes the shape of the quartet and doublet PESs, we carried out single-point UCCSD(T) calculations for all species on both PESs at the UB3LYP optimized geometries with the same basis set. The calculated relative energies by the two methods are collected in Table 1. From Table 1, one can see first that the relative energies on the same PES calculated by two methods are close to each other. For example, the barriers of the various steps on the quartet surface obtained by UB3LYP and UCCSD(T) methods are 0.9 and 1.6 ($^4$**2** → $^4$**3**), 29.2 and 29.0 ($^4$**3** → $^4$**7**), 9.7 and 3.5 ($^4$**7** → $^4$**8**), 32.7 and 34.9 ($^4$**8** → $^4$**9**), and 48.9 and 44.3 kcal/mol ($^4$**9** → $^4$**10**), respectively. Second, the differences between the doublet−quartet energy gaps calculated by the two methods are no more than 5.5 kcal/mol. Thus, the energies of the PESs with different spin states captured by the selected method is fairly in accord with that calculated by the UCCSD(T) method. This result provides us further confidence that the selected method with the selected basis set is reasonably accurate for describing the studied reaction systems.

**Table 1. Relative Energies $\Delta E_{Elec}$ (kcal/mol) of Stationary Points Calculated with UB3LYP and UCCSD(T) Methods on the Potential Energy Surfaces of the Reaction $OsO^+ + CH_4 \rightarrow OsCH_2^+ + H_2O$ in the Quartet and Doublet States[a]**

| species | quartet | doublet | $\Delta E_{DQ}$[b] |
|---|---|---|---|
| $OsO^+ + CH_4$ | 0.0[c] (0.0[d]) | 8.7 (12.1) | 8.7 (12.1) |
| **2** | −27.3 (−25.2) | −27.3 (−19.7) | 0.0 (5.5) |
| **TS2/3** | −26.4 (−23.6) | −27.2 (−21.4) | −0.8 (2.2) |
| **3** | −44.4 (−41.1) | −50.3 (−45.1) | −5.9 (−4.0) |
| **TS3/7** | −15.2 (−12.1) | −8.5 (−0.8) | 6.7 (11.3) |
| **7** | −52.7 (−45.9) | −50.4 (−44.9) | 2.3 (1.0) |
| **TS7/8** | −43.0 (−42.4) | −49.4 (−45.3) | −6.4 (−2.9) |
| **8** | −45.8 (−45.4) | −63.0 (−58.1) | −17.2 (−12.7) |
| **TS8/9** | −13.1 (−10.5) | −26.0 (−23.8) | −12.9 (−13.3) |
| **9** | −55.7 (−55.8) | −44.1 (−42.8) | 11.6 (13.0) |
| $OsCH_2^+ + H_2O$ | −6.8 (−11.5) | 0.0 (−1.1) | 6.8 (10.4) |

[a] Single point UCCSD(T) calculations are performed at UB3LYP optimized geometries, and the results are given in parentheses. [b] $\Delta E_{DQ} = \Delta E_{elec}$(doublet) − $\Delta E_{elec}$(quartet). [c] Absolute energy $E$ = −206.372369 au. [d] Absolute energy $E$ = −205.649208 au.

**3.2. Reaction of $OsO_2^+$ with Methane.** Similar to the reaction of $OsO^+$ with methane, there are three thermodynamically possible reaction channels for $OsO_2^+$ with methane. One is the dehydration process, which was observed experimentally, and the others are the dehydrogenation channel and the generation of the methyl radical, which were not found.

The calculated potential energy profiles of the dehydration reaction and the dehydrogenation channel are given in Figure 3. The optimized geometries for all stationary points on the quartet and doublet potential energy profiles are presented in Figure 4.

**3.2.1. $OsO_2^+ + CH_4 \rightarrow OOs(CH_2)^+ + H_2O$.** As shown in Figure 3a, the sextet PES locates much above the other two surfaces, but the doublet and quartet surfaces may intercross at the entrance and exit channels. For the intermediate species, their doublet states are significantly lower in energy than the corresponding quartet states. Since the transition state $^4$**TS13/14** is isoenergetic to the ground-state reactants ($^4OsO_2^+$ and $CH_4$), and the change of Gibbs free energy from the reactants to $^4$**TS13/14** is 8.4 kcal/mol, the reaction may not proceed on the quartet surface. Thus we will mainly focus on the doublet pathway in the following discussions.

The reaction starts on the quartet surface. The ground state of the reactant $OsO_2^+$ is a quartet state ($^4$**11**), which lies 15.2 and 29.3 kcal/mol below the correspond-

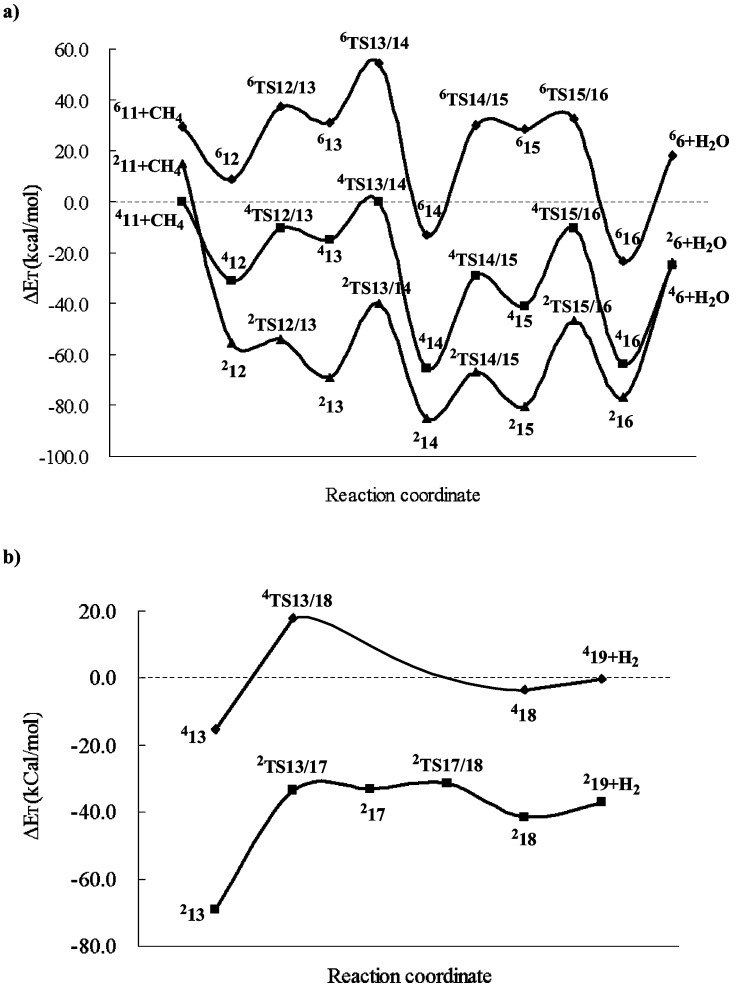


**Figure 3.** UB3LYP potential energy profiles of the reactions (a) $OsO_2^+ + CH_4 \rightarrow OOsCH_2^+ + H_2O$ in the sextet, quartet, and doublet states, and (b) $OsO_2^+ + CH_4 \rightarrow OOs(O)CH_2^+ + H_2$ in the quartet and doublet states. The early part of the pathway b is the same as that of the pathway a. For all species, the energies ($E_T$) are the sum of electronic energies and zero-point vibrational energies.



ing doublet and sextet species, respectively. The first step of the reaction is the formation of an electrostatic encounter complex $(CH_4)OsO_2^+$ ($^2$**12**). $^2$**12** is 24.4 and 64.1 kcal/mol lower in energy than the corresponding quartet and sextet species, respectively. This result suggests a possible spin inversion in the entrance channel. $^2$**12** has an $\eta^2$-C,H coordination mode, in which one of four C−H bonds is lengthened from 1.091 Å in free methane calculated at the same level to 1.197 Å, and the distance between Os and the closed hydrogen atom is 1.845 Å. The very strong α-agostic interaction[46] between Os and methane makes the formation of $^2$**12** strongly exothermic by 55.5 kcal/mol relative to the reactants $^4$**11** + $CH_4$; thus the formation of $^2$**12** is very facile with no barrier. From $^2$**12** to $^2$**13**, the first C−H bond of methane oxidatively adds to Os through the transition state $^2$**TS12/13** with a low barrier of 1.3 kcal/mol. $^2$**TS12/13** is a typical three-centered "late" transition state. The exothermicity of this step is 13.6 kcal/mol. In $^2$**13**, the calculated bond lengths suggest that the bonds Os−H1 and Os−C are typical covalent single bonds. The next step is the migration of H1 from Os to the nearby oxygen to yield the hydroxyl complex $OOs(OH)(CH_3)^+$ ($^2$**14**) via $^2$**TS13/14**. This step is exothermic by 15.9 kcal/mol with a barrier of 29.1 kcal/mol. From $^2$**14**, the reaction may go further along two directions. One direction is toward the elimination of the methyl ligand to give $^1$**15′** + $^\bullet CH_3$, which is endothermic by 79.5 kcal/mol. Following another direction, the second C−H bond of methane oxidatively adds to the metal to form the intermediate $OOs(H)(OH)(CH_2)^+$ ($^2$**15**). Then a reductive elimination step with H2 shifting from Os to the newly formed hydroxyl ligand occurs, forming a water-coordinated complex $OOs(H_2O)(CH_2)^+$ ($^2$**16**). The step from $^2$**14** to $^2$**15** goes over a barrier ($^2$**TS14/15**) of 18.2 kcal/mol, and it is endothermic by 4.7 kcal/mol. The barrier (via $^2$**TS15/16**) and the endothermicity for the subsequent step are 33.8 and 3.4 kcal/mol, respectively. Numerous trials to look for a four-membered transition state from $^2$**14** to $^2$**16**, in which a hydrogen atom in the methyl ligand migrates to the oxygen of the hydroxyl ligand, failed. Finally, $^2$**16** releases the water to give the final products $OOs(CH_2)^+$ (**6**) + $H_2O$. Since the ground state of **6** is its quartet state, the reaction may jump back from the doublet surface to the quartet one near the exit channel. If this happens, the final step requires 52.2 kcal/mol, and the entire reaction for dehydration of methane by $OsO_2^+$ is exothermic by about 24.0 kcal/

(46) (a) Brookhart, M.; Green, M. L. H. *J. Organomet. Chem.* **1983**, *250*, 395−408. (b) Eisenstein, O.; Jean, Y. *J. Am. Chem. Soc.* **1985**, *107*, 1177−1186. (c) Calhorda, M. J.; Simões, J. A. M. *Organometallics* **1987**, *6*, 1188−1190.

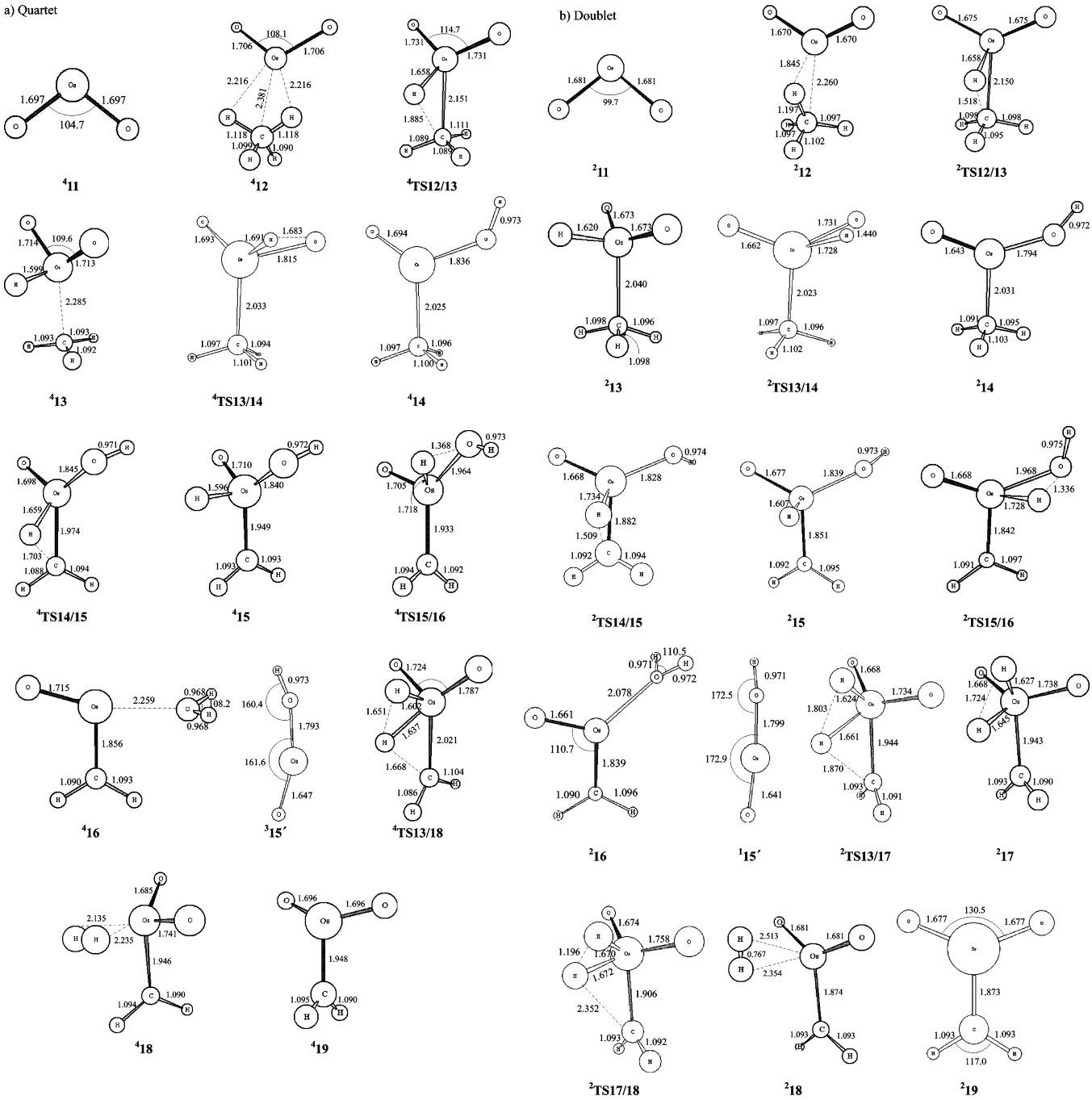


**Figure 4.** Optimized geometries for the stationary points of the reactions $OsO_2^+ + CH_4 \rightarrow OOsCH_2^+ + H_2O$ and $OsO_2^+ + CH_4 \rightarrow OOs(O)CH_2^+ + H_2$ in the quartet (a) and doublet (b) states.

mol. However, since the energy difference between **$^4$6** and **$^2$6** is only 0.7 kcal/mol, the final products may exist in two spin states.

**3.2.2. $OsO_2^+ + CH_4 \rightarrow OOs(O)CH_2^+ + H_2$.** For this pathway, since the sextet PES is much higher in energy than the quartet and doublet ones, we only provide the quartet and doublet PESs in Figure 3b and the optimized geometries of the corresponding species in Figure 4, respectively.

As seen from Figure 3b, the PESs of the dehydrogenation pathway diverge from those of the dehydration pathway after the intermediate **13** is formed, and the doublet surface is significantly lower in energy than the quartet surface except that the ground state of the initial reactant **11** is a quartet state. We will focus on the discussion on this PES. Along the dehydrogenation pathway, the subsequent step is the oxidative addition of the C−H2 bond of methane to the metal via **$^2$TS13/17** to form the dihydride intermediate $(O)_2Os(H)_2CH_2^+$ (**$^2$17**). The transition state **$^2$TS13/17** is very late, and this step has a barrier of 35.8 kcal/mol and is endothermic by 36.1 kcal/mol. Next, two hydrides reductively eliminate readily to yield the dihydrogen complex $(O)_2Os(H_2)CH_2^+$ (**$^2$18**) via **$^2$TS17/18**. From Figure 4, one can see that in **$^2$18** the H1−H2 distance (0.767Å) is close to that in free $H_2$, and two hydrogens are 2.513 and 2.354 Å from the metal, respectively, indicating that **$^2$18** is a typical dihydrogen complex. Finally, the elimination of $H_2$ can occur readily to produce the final products $Os(O)_2CH_2^+$ (**$^2$19**) and $H_2O$. In contrast, on the quartet

PES, the dihydrogen complex $^4$**18** is formed directly from $^4$**13** via $^4$**TS13/18** by the oxidative addition of the C−H2 bond to Os without the formation of the dihydride intermediate.

As shown in Figure 3, for the dehydrogenation of methane by $OsO_2^+$, the ground state of the initial reactant $OsO_2^+$ is a quartet state, and all the subsequent stationary points have the lowest energy in the doublet state. Thus, the quartet and doublet PESs may intercross somewhere before the intermediate **12**. The reaction starts from the quartet state and then may proceed on the doublet pathway; the overall reaction would be exothermic by 36.9 kcal/mol. The rate-limiting step is the oxidative addition of the C−H2 bond (from $^2$**13** to $^2$**17** through $^2$**TS13/17**) with a barrier of 35.8 kcal/mol.

Now we compare the dehydration channel with the dehydrogenation channel. Along the dehydration direction, the reaction is exothermic by about 24.0 kcal/mol, and the rate-determining steps are the two hydride transfer steps and the loss of the water ligand from $^2$**16**. While along the dehydrogenation direction, the reaction has the exothermicity of 36.9 kcal/mol, and the rate-limiting step is the activation of the second C−H bond of methane. Thus, the dehydrogenation channel is thermodynamically favorable. However, since along the dehydration direction the barrier of the first hydride transfer step (from **13** to **14**) is 6.8 kcal/mol lower in energy than that of the second C−H activation (from **13** to **17**) on the dehydrogenation pathway, the dehydration channel is kinetically preferred and should account for the experimental observation. Indeed, the reaction of methane with $OsO_2^+$ was found experimentally to occur along the dehydration pathway.

To summarize the above discussions, the reaction of methane by $OsO_2^+$ prefers to go through the dehydration channel (the reaction channel with the formation of methyl radical is much higher in energy than the dehydration and dehydrogenation channels). If the reaction involves the spin inversion at the entrance and exit channels, the minimum energy reaction path is $^4$-$OsO_2^+ + CH_4 \rightarrow {}^2O(O)OsCH_4^+$ ($^2$**12**) $\rightarrow {}^2O(O)Os(H)CH_3^+$ ($^2$**13**) $\rightarrow {}^2O(HO)Os(CH_3)^+$ ($^2$**14**) $\rightarrow {}^2O(HO)Os(H)(CH_2)^+$ ($^2$**15**) $\rightarrow {}^2OOs(H_2O)(CH_2)^+$ ($^2$**16**) $\rightarrow {}^4OOs(CH_2)^+$ ($^4$**6**) + $H_2O$.

**3.3. Reaction of $OsO_3^+$ with Methane.** Thermodynamically, the reaction of $OsO_3^+$ with methane also has two possible reaction channels, i.e., the dehydration process and the process generating methyl radicals, but the dehydrogenation process producing $Os(O)_3(CH_2)^+$ (**25**) and $H_2$ is calculated to have a free energy change of +7.0 kcal/mol at room temperature and thus is thermodynamically very unfavorable. Next we will discuss the former two possible reaction channels. Since the sextet and quartet surfaces are much higher in energy than the doublet surface, only the doublet potential energy profile is displayed in Figure 5. The optimized geometries for all species are shown in Figure 6.

As shown in Figures 5 and 6, the first step of the reaction, the formation of the electrostatic complex $^2$**21**, is exothermic by 17.9 kcal/mol relative to the doublet reactants $OsO_3^+$ ($^2$**20**) + $CH_4$. The next step is the oxidative addition of the first C−H bond of methane to

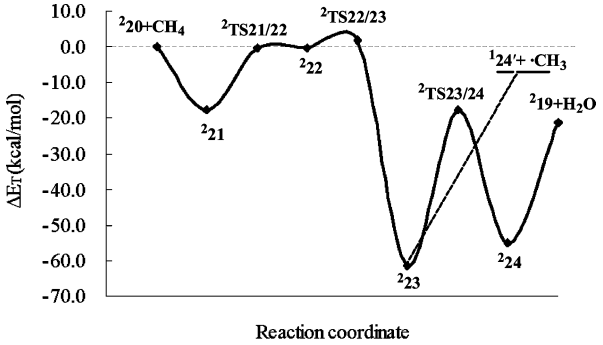


**Figure 5.** UB3LYP potential energy profile of the reaction of $OsO_3^+$ with $CH_4$ in the doublet state. For all species, the energies ($E_T$) are the sum of electronic energies and zero-point vibrational energies.

Os to yield $^2$**22** via the transition state $^2$**TS21/22**. The Os−H1 and Os−C distances of 1.652 and 2.335 Å in $^2$**TS21/22**, respectively, are very close to the corresponding distances in $^2$**22**, showing that $^2$**TS21/22** is a very "late" transition state. This step involves a barrier of 17.5 kcal/mol and is endothermic by 17.4 kcal/mol. As shown in Figure 6, the Os−C distance in $^2$**22** is 2.382 Å, indicating a weak interaction between the methyl group and the metal center. Considering that the maximum formal oxidation state of Os is +8, it is understandable that the Os−C bond in $^2$**22** is not a typical covalent bond, otherwise the oxidation state of Os would be +9 in $^2$**22**. Our calculations show that the loss of the methyl group from $^2$**22** to generate the species $Os(O)_3(H)^+$ is endothermic by 23.5 kcal/mol. To make the reaction go along the dehydration direction, the next step must be the migration of the hydride ligand to one oxo ligand (from **22** to **23**) to lower the formal oxidation state of Os from +8 in $^2$**22** to +7 in $^2$**23**. As shown in Figure 6, the transition state in this step, $^2$**TS22/23**, is very "early", leading to a small activation energy of 2.4 kcal/mol. The structure of $^2$**23** clearly shows that the Os−C bond is a typical covalent single bond, being much stronger than that in $^2$**22**. As a consequence, the step from $^2$**22** to $^2$**23** is strongly exothermic by 61.1 kcal/mol. From $^2$**23**, the reaction may go further toward two different channels. The first one is the loss of the methyl group to give the product $^1$**24′**. This step requires 59.9 kcal/mol. The second pathway is the migration of one hydrogen atom of the methyl ligand to the oxygen atom of the hydroxyl ligand via the four-centered transition state $^2$**TS23/24**, yielding the complex $^2$**24**, in which a water molecule is coordinated to the metal. The calculated barrier of this step is 43.8 kcal/mol. The final step is the release of $H_2O$ from $^2$**24** to generate the final products $^2OOs(O)CH_2^+$ ($^2$**19**) + $H_2O$, which requires 33.8 kcal/mol.

To conclude, for the reaction of $OsO_3^+$ with methane, the channel with the formation of the methyl radical and $^1$**24′** is exothermic by 1.73 kcal/mol, and the dehydration channel is exothermic by 21.2 kcal/mol. However, since the species $^2$**TS21/22** and $^2$**22** are nearly isoenergetic to the initial reactants $^2OsO_3^+ + CH_4$, and their Gibbs free energies are about 8.0 kcal/mol above that of the reactants, the reactions along both pathways are kinetically unfavorable at room temperature. This result is in accord with the experimental observation

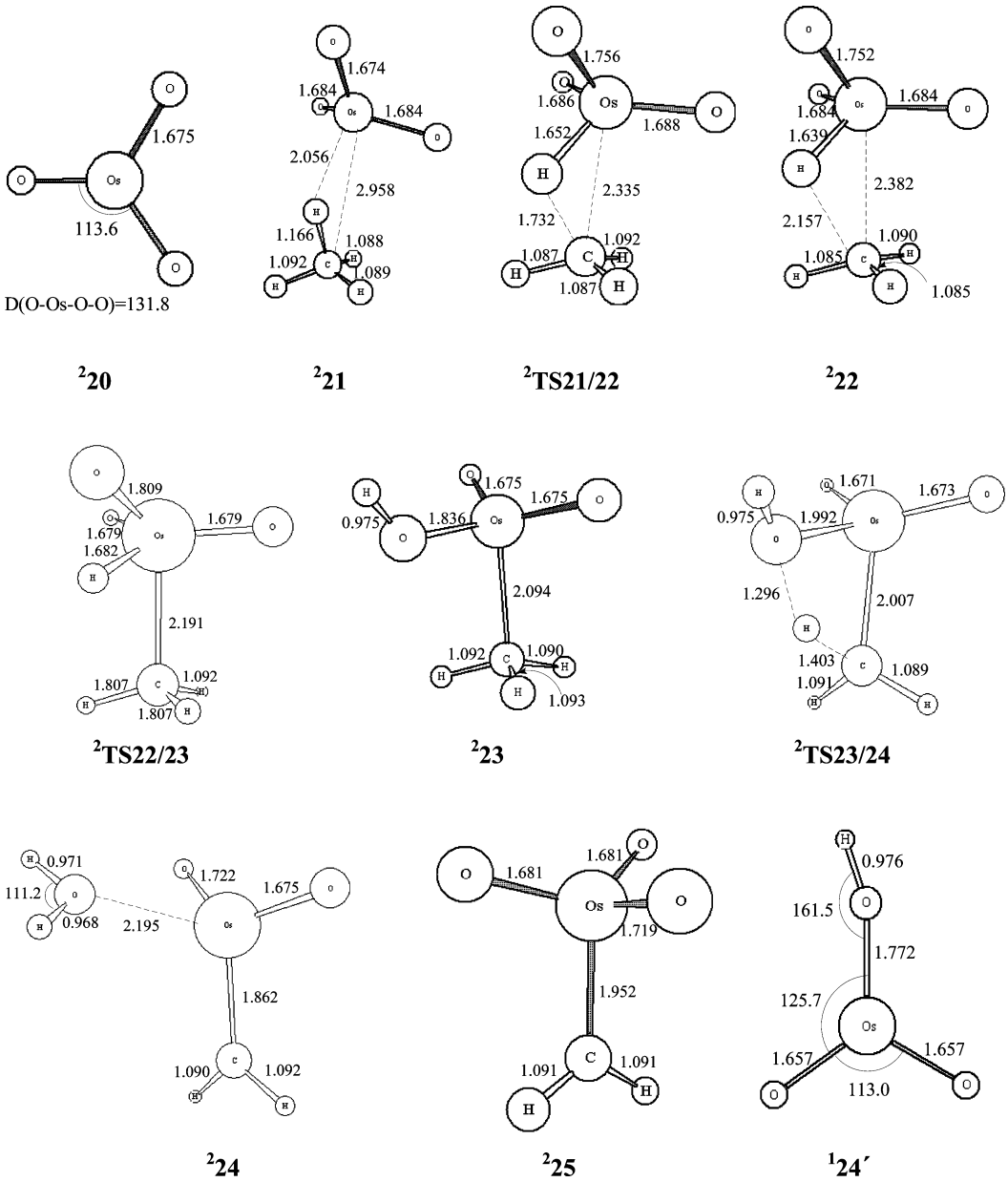


**Figure 6.** Optimized geometries for the stationary points of the reaction $OsO_3^+$ with methane in the doublet state.



that $OsO_3^+$ is unreactive to methane under the experimental conditions.

**3.4. Reaction of $OsO_4^+$ with Methane.** Before we discuss the reaction of $OsO_4^+$ with methane, let us take a look at the geometry and electronic structure of $OsO_4^+$. Our calculations suggest that the global minimum of $OsO_4^+$ is $^2$**26**. As shown in Figure 7, $^2$**26** is of nearly $T_d$ symmetry. The four Os−O bonds have the same length, but there are two kinds of O−Os−O angles (108.5° and 111.4°). Since the formal oxidation state of Os is at most +8, the Os−O bond in $^2$**26** cannot be a typical double bond, otherwise Os would be formally +9 in $^2$**26**. This prediction is confirmed by the calculated Os−O bond lengths in $^2$**26**, which are significantly longer than those in the series $OsO_n^+$ ($n$ = 1−3). Thus, $^2$**26** may be considered as an oxygen-centered cation radical. In addition, we also located another low-energy minimum of $OsO_4^+$, $^2$**27**. This species is only 4.2 kcal/mol higher in energy than $^2$**26** and can be described as a dioxygen complex, $Os(O)_2(O_2)^+$, as seen from its structure (in Figure 7). For these two species, their quartet and sextet states were found to be much higher in energy; thus we will only discuss the reactivity of $^2$**26** and $^2$**27** toward methane.

For the reaction of $^2$**26** with methane, since Os already reaches its highest oxidation state in $^2$**26**, the direct hydrogen atom abstraction process to produce methyl radicals is the most probable reaction channel. Indeed, this channel was observed experimentally. With $^2$**26** as the reactant, the calculated potential energy profile is shown in Figure 8. For the reactant $^2$**27**, since the oxidation state of Os is formally +5, the direct hydrogen atom abstraction process and the oxidative addition process of methane are two possible channels. We also investigated the potential energy profiles of these two pathways for the reaction of $^2$**27** with methane, and the results are briefly discussed in the following text. For both reactants, the optimized geometries of the stationary points are collected in Figure 7.

As shown in Figure 8, the first step of the reaction is the formation of the hydrogen atom abstraction intermediate, $^2$**28**. This is a barrierless process and is

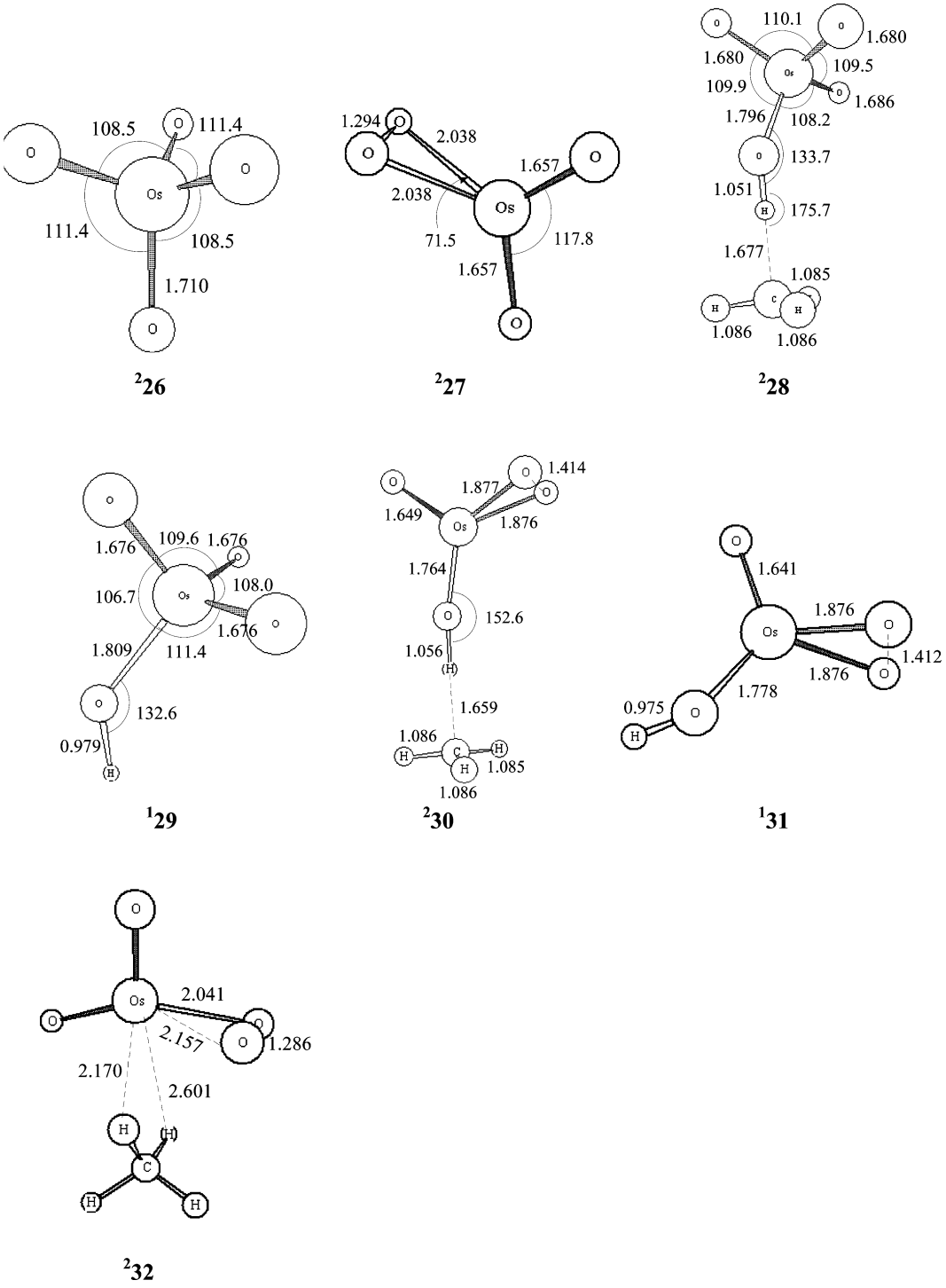


**Figure 7.** Optimized geometries for the stationary points of the reaction $OsO_4^+ + CH_4 \rightarrow Os(O)_3(OH)^+ + {}^\bullet CH_3$ in the doublet state.

strongly exothermic by 49.7 kcal/mol. In **$^2$28**, one can see that one of the C−H bonds of methane is almost broken, and the newly formed O−H bond is almost complete. The next step is the elimination of the methyl group from **$^2$28** to give the final products **$^1$29** + $^\bullet CH_3$, which requires 17.9 kcal/mol. Although we made many trials to look for the transition states for the hydrogen abstraction process of methane by **$^2$26** and for the loss of the methyl radical from **$^2$28**, no transition states were found for these two processes. The whole reaction is exothermic by 31.8 kcal/mol. Therefore, the hydrogen atom abstraction process of methane by **$^2$26** should be thermodynamically and kinetically accessible at room temperature, which agrees with the experimental observation.

In addition, we would like to mention briefly the reactivity of **$^2$27** toward methane. First, along the hydrogen atom abstraction channel, the intermediate **$^2$30** was located, which is 1.9 kcal/mol below the reactants **$^2$27** + $CH_4$. Then the leaving of the methyl group to generate **$^1$31** requires 16.1 kcal/mol. Since the Gibbs free energy change from the reactants to the products is +14.3 kcal/mol, this hydrogen atom abstraction process cannot take place at room temperature.

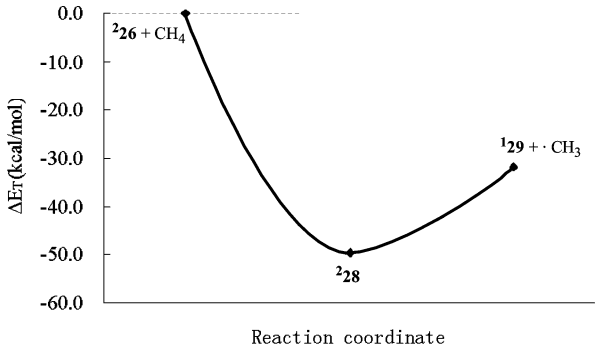


**Figure 8.** UB3LYP potential energy profile of the reaction $OsO_4^+ + CH_4 \rightarrow Os(O)_3(OH)^+ + {}^\bullet CH_3$ in the doublet state. For all species, the energies ($E_T$) are the sum of electronic energies and zero-point vibrational energies.

Second, one may wonder if methane can be readily activated by **$^2$27** via an oxidative addition step. Along this direction, the initial step would be the formation of the encounter complex **$^2$32**. However, due to the fact that this association step has a Gibbs free energy change of 4.3 kcal/mol, this process is not likely to occur at room temperature either.

To conclude, $OsO_4^+$ can react with methane readily through a direct hydrogen atom abstraction process. The whole reaction occurs on the doublet PES and is exothermic by 31.8 kcal/mol.

## 4. Conclusions

Systematic studies have been carried out to investigate the reactivity and mechanisms of gas-phase oxo osmium cations $OsO_n^+$ ($n = 1-4$) with methane via density functional calculations. The sextet, quartet, and doublet potential energy surfaces for each reaction have been explored in detail. The potential energy surfaces of $OsO_n^+$ ($n = 1, 2$) with methane are somewhat similar to each other, but they are significantly different from those of the reactions of $OsO_3^+$ and $OsO_4^+$ with methane. Specifically, the following conclusions can be drawn from the present calculations.

(a) For the reaction of $OsO^+$ with methane, the dehydrogenation channel is found to be thermodynamically and kinetically preferred. For $OsO_2^+$, our calculations show that the dehydration channel is kinetically preferred, despite the fact that the dehydrogenation channel is thermodynamically more favorable. In these two reactions, the minimum energy reaction path involves the crossings between the quartet and doublet surfaces at entrance and exit channels, respectively.

(b) The formal oxidation state of the Os center is a useful quantity for us to qualitatively understand the C−H activation of methane by $OsO_n^+$ ($n = 1-4$). To facilitate the activation of the first C−H bond of methane through an oxidative addition step, the formal oxidation state of the Os center is required to be no more than +6, since two covalent Os−C and Os−H bonds can then be formed in the oxidative addition intermediate (note that the maximum formal oxidation state of Os is +8). Thus, the first C−H bond of methane can be readily activated by $OsO^+$ and $OsO_2^+$, in which the oxidation state of Os is +3, and +5, respectively. But, this is not the case for $OsO_3^+$ and $OsO_4^+$. In $OsO_3^+$, the oxidation state of Os is already +7. So only a typical Os−H bond is formed in the oxidative addition intermediate $Os(O)_3(H)(CH_3)^+$, which has a relatively high energy. This accounts for the experimental observation that $OsO_3^+$ is unreactive to methane under the experimental condition. But for $OsO_4^+$, since the Os center is in its highest oxidation state, its reaction with methane must go through a direct hydrogen atom abstraction process, instead of the oxidative addition channel. The above simple analysis is supported by our detailed calculations.

**Acknowledgment.** This work was supported by the National Natural Science Foundation of China (Grant Nos. 20373022 and 20233020). We are grateful to the three referees for their pertinent comments and good suggestions concerning our original manuscript. Partial computations were carried out on the SGI Origin 3800 and Dawning 3000A at Nanjing University.

**Supporting Information Available:** This material is available free of charge via the Internet at http://pubs.acs.org.

OM049959B